JOURNAL OF AGRICULTURAL AND FOOD CHEMISTRY

High-Speed Assessment of Fat and Water Content Distribution in Fish Fillets Using Online Imaging Spectroscopy

GAMAL ELMASRY*,† AND JENS PETTER WOLD‡

Agricultural Engineering Department, Faculty of Agriculture, Suez Canal University, Ismailia, Egypt, and MATFORSK-Norwegian Food Research Institute, Osloveien 1, 1430 Ås, Norway

A nondestructive method using online spectral imaging has been developed for quantitative measurements of moisture and fat distribution in six species of fish fillets: Atlantic halibut (*Hippoglossus hippoglossus*), catfish (*Icatalurus punctatus*), cod (*Gadus morhua*), mackerel (*Scomber japonicus*), herring (*Clupea harengus*), and saithe (*Pollachius virens*). A spectral image cube was acquired for each fish fillet, and a subsampling approach for relating spectral and chemical features was applied. Spectral data was first analyzed by partial least-squares regression (PLSR), and then the regression coefficients were applied pixel-wise to convert the pixel spectra to a meaningful distribution map of moisture and fat contents. The resulting images are called "chemical images", which illustrate the distribution of fat and/or water content in the fillets. The pixel-wise prediction models for water and fat content had a correlation value of 0.94 with root-mean-square error estimated by a cross-validation (RMSECV) of 2.73% and a correlation value of 0.91 with RMSECV of 2.99%, respectively. This technique is suitable for high-speed assessment of quality parameters of biomaterials and should thus be implemented in industrial applications. The product could comprehensively be defined not only in terms of its external features such as size, shape, and color but also in terms of its chemical composition and its spatial distribution.

KEYWORDS: Fish fillet; spectral imaging; multivariate analysis; near-infrared spectroscopy; Atlantic halibut; catfish; cod; mackerel; herring; saithe

INTRODUCTION

The current demand for fish as food is systematically increasing (*1*), and future demand for fish will basically be determined by the number of consumers and their eating habits and disposable income as well as by fish prices (*2*). Quality assessment and documentation of chemical composition of the produce is important for both producers and consumers. All of these factors have underscored the need for implementing reliable, accurate, quick, nondestructive, and inexpensive online techniques for quality assessment and monitoring. Online quality monitoring systems may provide better means for sorting fish as well as provide better documentation of product quality for price differentiation and promotion.

During the past few decades a number of different techniques have been explored as possible instrumental methods for quality evaluation of fish. Spectroscopic analysis exploits the interaction of electromagnetic radiation with atoms and molecules to provide qualitative and quantitative chemical and physical information that is contained within the wavelength spectrum that is either absorbed or emitted. Among these spectroscopic techniques, near-infrared (NIR) spectroscopy is one of the most successful within the food industry. The absorption bands seen in this spectral range arise from overtones and combination bands of O−H, N−H, C−H, and S−H stretching and bending vibrations which enable qualitative and quantitative assessment of some of chemical and physical features (*3–6*). Near-infrared spectroscopy fulfils the demand of a rapid, accurate, and simple method for documentation of chemical composition in food and beverage analysis (*7*). The technique ability of quickly incorporating the advances in correlated fields, such as spectral imaging and optics, ensures it an extensive and fruitful field for research and development (*4*).

Spectral imaging or imaging spectroscopy combines two well-known methodologies, namely spectroscopy and imaging, to provide a new advantageous tool (*8*). The combination of these two techniques is, however, not trivial, mainly because it requires creating a three-dimensional (3D) data set that contains many images of the same object, where each one of them is measured at a different wavelength. Each point in the cube represents a single number, and the spectral image is described as $I(x,y,\lambda)$. It can be viewed either as an image $I(x,y)$ at each wavelength λ, or as a spectrum $I(\lambda)$ at every pixel (x,y) (*5, 9*).

* Corresponding author: Tel: +20120058048, fax: +20643320793, e-mail: g.elmasry@scuegypt.edu.eg.
† Suez Canal University.
‡ MATFORSK- Norwegian Food Research Institute.

10.1021/jf801074s CCC: $40.75
Published on Web 07/26/2008

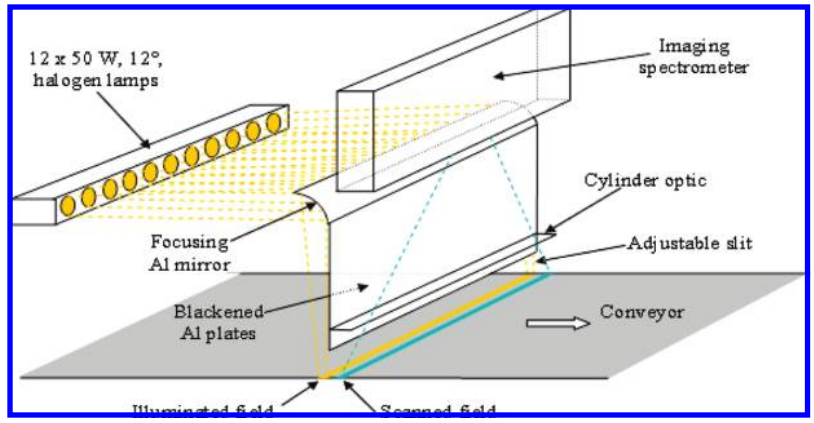

Figure 1. Layout of the main configuration of the NIR spectral imaging system.

Spectral imaging is a relatively new technique, and its full potential has yet to be exploited. The spectral information allows detecting and distinguishing among many different objects even if they have a similar color or overlapping spectra. This permits one to label different entities in a sample simultaneously and to quantitatively analyze each entity. The advantage is that the spatial distribution of chemical composition in the product can be obtained, not just the bulk composition (*10*). Accordingly, extensive research and development work utilizing spectral imaging techniques have been undertaken in various aspects of food processing, such as inspection of poultry carcasses (*11, 12*), quality determination of some agricultural products (*13–16*), detection of nematodes in fish fillets (*8*), and foreign substances in fruits (*17*). In addition, a NIR imaging spectroscopy was used to visualize sugar distribution in melons, by producing a sugar distribution map where the sugar content was visualized by different colors (*18, 19*).

Spectral imaging technology has to a very limited extent been directly implemented in online systems for automated quality detection because its time requirements for image acquisition and analysis are too great (*20*). To overcome this problem, the high dimensionality of the spectral data at numerous wavelengths is first reduced to few optimal wavelengths. Then, a multispectral imaging system is formed with a reference of these selected wavelengths for rapid online assessments (*21*).

Fat and water contents are key quality parameters of fatty fishes such as salmon, mackerel, herring, and tuna and influence sensory, nutritional, and processing properties (*22*), Today's chemical methods for fat determination are highly destructive and time-consuming and require use of hazardous chemicals that may be harmful to analysts and the environment. Screening of every single fillet requires an online method for fat and water determination (*10*). Such a method enables optimized processing of the raw material, correct pricing, and labeling and gives the opportunity to sort fish with different fat content according to market requirements and product specifications.

The main aim of the present study was to establish a nondestructive system using an NIR interactance spectral imaging technique to determine water and fat content distribution in the fillets of six fish species in real time. The work was carried out by (1) applying a NIR spectral imaging system with a spectral region of 760−1040 nm, (2) building robust calibration models using partial least-squares regression (PLSR) to quantitatively relate chemical and spectral information, and (3) development of image processing algorithms for mapping the concentration of a given constituent (fat or water content) to form chemical images.

MATERIALS AND METHODS

Fish Fillets. Forty fish fillets of six different species: Atlantic halibut (5 fillets), Catfish (5 fillets), Cod (5 fillets), Saithe (5 fillets), mackerel (10 fillets), and Herring (10 fillets) were purchased from local fish retailer (Fiskemat AS, Oslo, Norway). The fish fillets were fresh and of superior quality.

Spectral Image Acquisition. A spectral image of each fillet was acquired using the NIR spectral imaging scanner Qmonitor (Qvision AS, Oslo, Norway). This industrial online scanner records spectral images in the visible and near-infrared range of 460−1040 nm with a spectral resolution of approximately 20 nm at the speed of 10 000 spectra per second. The pixel absorption spectra in the NIR range (760−1040 nm) consist of 15 wavelengths. The system is thoroughly described by Wold et al. (*10*). **Figure 1** shows how the system is designed to measure in the interactance mode. The light is focused along a line across the conveyor belt. A metal plate is used to shield the detector from unwanted reflected light from the fish surface. In that way, it is assured that the detected light has been transmitted into the fish and then back scattered to the surface, i.e. only the light that has traversed the interior of the fish will be analyzed. Interactance thus probes deeper into the fillet compared to reflectance and suppresses surface effects. Interactance has a practical advantage over transmission that both illumination and detection are on the same side of the sample. This reduces the influence of thickness considerably and provides a fairly clear measurement situation.

Fish fillets were put on the conveyor belt one by one and moved at a speed of approximately 0.1 ms^{-1}, which resulted in a spatial resolution of 0.3 mm along the conveyor belt. Image size varied according to the length of the fish. The fish was scanned line-by-line to collect the entire spectral image. The data is therefore collected as $I(x,\lambda)$ and then scanned along the conveyor belt movement direction (y direction). Distance between the fish and the lower edge of the light shield was minimized to avoid varying levels of stray light and surface reflectance. The minimum distance between the thickest part of the fish and the shield was approximately 1 cm, while the maximum distance was approximately 4−5 cm, depending on the thickness of the fillet. Matlab 6.4 (The Mathworks Inc., Natick, MA, USA) was used for controlling the unit, image recording, and real-time data collection.

Subsampling for Reference Analysis. The fat content can vary a lot within the same fillet, and local concentrations could be much higher or lower than the average fat content. To obtain NIR calibrations that could be applied pixel-wise, it was important to include an appropriate span of fat and water concentrations in the calibration samples. This was done by cutting out five cylindrical subsamples (each approximately 10 mm in diameter) from the thicker loin, belly, tail, and lateral 'notch' parts of every fillet, resulting in a total of 150 subsamples. The subsamples were picked from different locations of the fillets, which spanned the fat and water content, aiming to collect samples with concentrations evenly distributed over the full chemical range of fat and water.

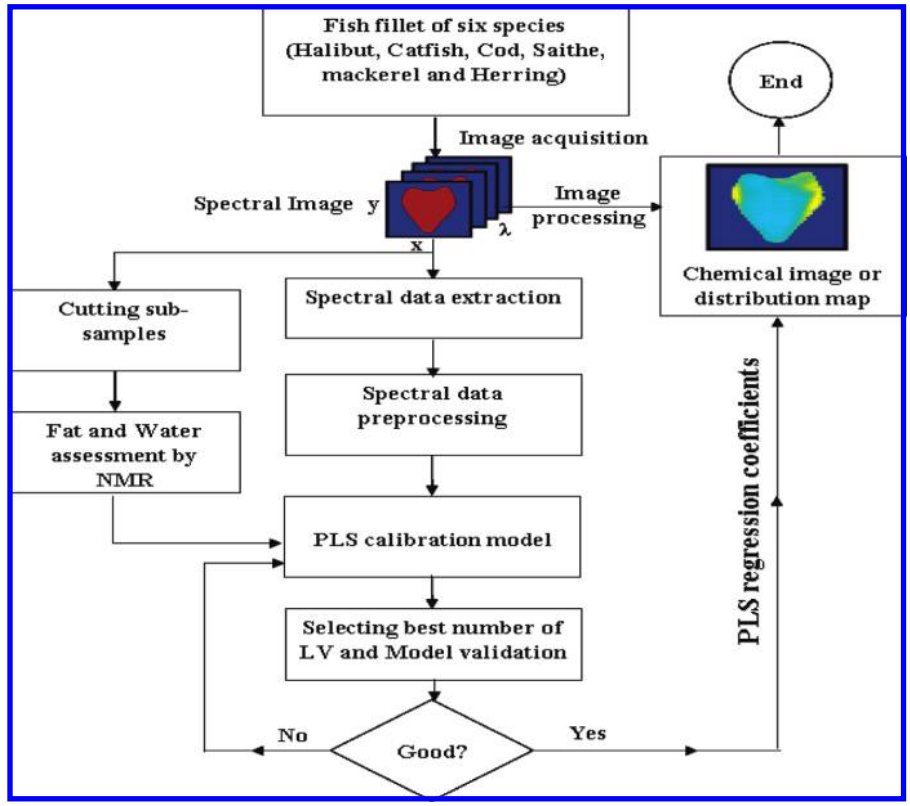

Figure 2. Key steps for building chemical images (distribution maps).

Reference Analysis of Subsamples. Water and fat content in subsamples were determined by low field nuclear magnetic resonance (LF-NMR). In NMR, the measured signal is proportional to the total amount of hydrogen atoms in the samples. The method used was the one-shot method, which is based on measurements of relaxation times. The signals originating from water and fat can be separated by applying a multipulsed field gradient spin echo experiment, taking advantage of the difference in proton mobility (*23*). The instrument used was Maran Ultra Resonance (Oxford Instruments, Oxfordshire, UK) equipped with a gradient probe. The subsamples were placed in 18 mm NMR tubes and heated to 40 °C to ensure a liquid fat phase to acquire the total fat signal. Calibration of the NMR system was done on a sample of known weight containing 100% fish oil. The weight of each subsample was recorded to calculate the percentage of fat and water.

Extraction of Calibration Spectra. One spectral image is a group of images where each pixel represents a spectrum for that specific point. To establish the spectral calibration set, NIR spectra from the image pixels corresponding to the circular area where the reference subsamples had been collected, were extracted. Pixel spectra within each circular region were averaged. This resulted in an X-matrix of 150 spectra. All extraction routines and pixel-based predictions were programmed in Matlab 7.3 (The Mathworks Inc.).

Data Analysis and Calibration. Partial least-squares regression (PLSR) can be considered as a standard calibration technique for NIR data. The main advantage of this technique is to avoid colinearity problems, permitting work with a number of variables that is greater than the number of samples. PLSR finds a mathematical relationship between a set of independent variables, the X-matrix ($N_{samples} \times K_{wavelengths}$), and the dependent variable, the Y-matrix ($N_{samples} \times 1$). Where the X-matrix represents the spectra or absorbance values at the 15 wavelengths (k) for the 150 subsamples (N), whereas, the Y-matrix represents the concentration of fat or water content in the subsamples. Separate models were made for fat and water. X and Y matrices were preprocessed by mean-centering prior to calibration.

The optimal number of latent variables (LV) for establishing the calibration model was determined using the minimum value of predicted residual error sum of squares (PRESS). Full cross-validation was used for all models to provide a predicted value for each sample ($\hat{y}_i$), which was then compared to the reference value (y_i) for all subsamples. Cross-validation removes one sample or a subset of samples from the calibration data, and then constructs a model with the remaining data. The samples left out then have their values predicted by the model. The procedure is repeated for each sample or subset of samples, and a root-mean-square error estimated by cross-validation (RMSECV) is computed as:

$$\mathrm{RMSECV} = \sqrt{\frac{1}{N}\sum_{i=1}^{N}(\hat{y}_i - y_i)^2}$$

Calibration analysis was performed with Matlab 7.3 (The Mathworks Inc.) and the PLS toolbox (Eigenvector Research, Inc., Wenatchee, WA).

Mapping of Water and Fat Content. The PLS regression models were used to predict water and fat concentrations in each pixel of the spectral image. This was done by calculating the dot product between each pixel spectrum and the coefficient vector obtained from the PLSR model. The resulting chemical image is displayed in colors, where the colors represent different concentrations. The key steps for creating these chemical images are depicted in the flowchart shown in **Figure 2**.

Table 1. Moisture and Fat Content in Fish Fillets

	water, %			fat, %		
	min	max	mean ± SD	min	max	mean ± SD
Atlantic halibut	56.48	85.41	74.50 ± 7.63	1.39	18.79	10.14 ± 5.67
catfish	60.35	75.88	72.60 ± 3.91	5.06	22.77	9.15 ± 4.10
cod	77.53	81.52	80.20 ± 1.08	0.12	0.71	0.39 ± 0.15
mackerel	56.45	69.13	63.84 ± 3.57	10.46	22.92	14.74 ± 3.21
herring	62.82	71.97	67.44 ± 2.20	9.55	17.85	13.09 ± 2.21
saithe	77.04	81.00	78.99 ± 1.05	0.24	0.62	0.37 ± 0.11

RESULTS AND DISCUSSION

Reference Analyses. Table 1 shows an overview of moisture and fat contents of subsamples from the six fish species measured by NMR. The minimum and maximum values of fat

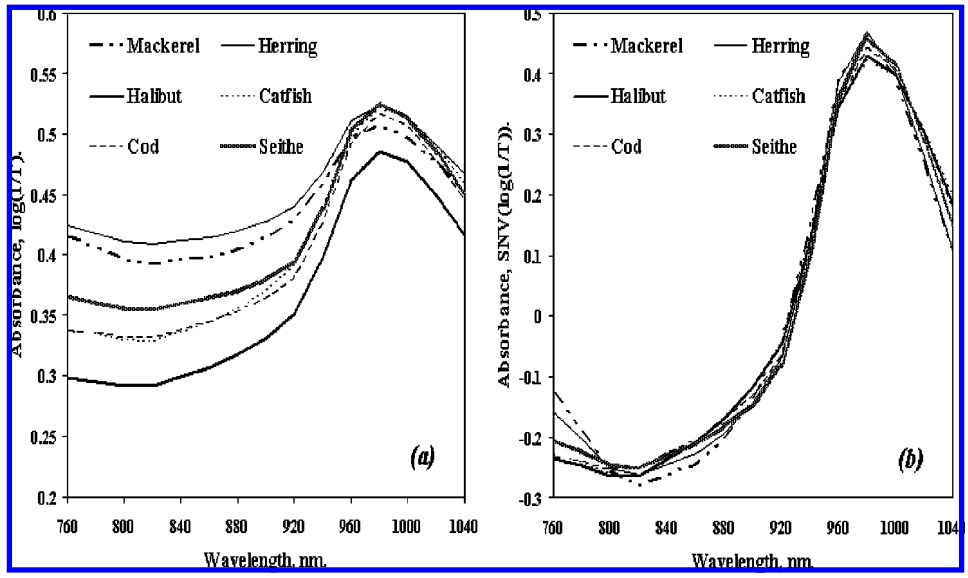

Figure 3. Average NIR interactance spectra of mackerel (14.74% fat), herring (13.09% fat), catfish (9.15% fat), halibut (10.14% fat), cod (0.39% fat), and saithe (0.37% fat): (**a**) absorbance spectra; (**b**) corrected absorbance spectra by the standard normal variate (SNV) preprocessing method.

and moisture content within each species demonstrate that the concentrations varied a lot between different parts of the fillets. In particular, this was the case for Atlantic halibut, catfish, and mackerel where standard deviation values were high. The water content of the tested samples ranged from 56.45 (found in mackerel) to 85.41% (found in Atlantic halibut). Meanwhile, the fat content ranged from 0.12 (found in cod) to 22.92% (found in mackerel). A wide distribution in concentrations was obtained, which was beneficial to produce stable calibration models. Cross-correlation between fat and water was −0.91.

Spectral Features of Fish Fillets. Figure 3a) shows the average NIR interactance spectra from subsamples of different fish species. The absorbance spectra from the fish fillets were rather smooth across the spectral region. The broad peak at about 980 nm is assigned to the O−H stretch second overtone in H_2O. Fat has an absorbance peak at 930 nm corresponding to the third overtone C−H stretch in the methylene group of fat (*24*), which is difficult to discern in the figure. The prominent offset variation between the spectra is mainly due to light scattering phenomena caused by varying the distance between fish and the light-blocking shield (due to varying fillet thickness). Herring and mackerel were the thinnest fillets, having spectra with low contrast, i.e. the intensity ratio between 980 and 820 nm is low, whereas the thicker halibut and catfish had spectra with considerable higher contrast. The longer the distance between the sample and the light-blocking shield, the more detected signal from surface-reflected light and correspondingly less interactance light. Some details in the spectra are easier to see in **Figure 3b**) which demonstrates the same spectra after correction by the standard normal variate (SNV) preprocessing method. In herring, mackerel, and saithe there is slightly higher absorbance from 800 nm toward 760 nm. This is due to the darker color of these species. The fat absorbance at 930 nm can be seen as different levels in the spectra. A quite clear trend is that samples with high fat content have high values in this region, except for the herring. The shown spectra illustrate the complexity of the data.

Modeling of Fat and Water Content in Fish Fillets by PLSR. The results of PLSR models for fat and water are shown in **Table 2** and **Figure 4**. The quality of the calibration models was evaluated by the root-mean-square error of calibration (RMSEC), root-mean-square error estimated by cross-validation (RMSECV), and the correlation coefficient (*r*) between the predicted and measured values. A good model should have a low RMSEC, a low RMSECV, a high correlation coefficient,

Table 2. Pixel-Based PLSR Models for Water and Fat in Fish Fillets

	PLS model			
constituent	latent variables (LV)	correlation coefficient, *r*	RMSEC	RMSECV
water	8	0.94	2.45	2.73
fat	6	0.91	2.70	2.99

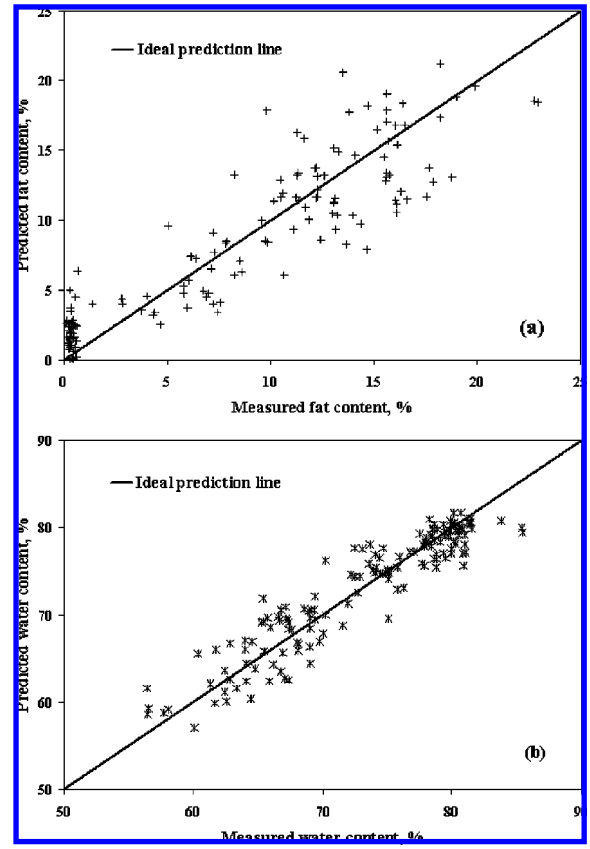

Figure 4. Measured and predicted fat (**a**) and water (**b**) contents by PLSR models.

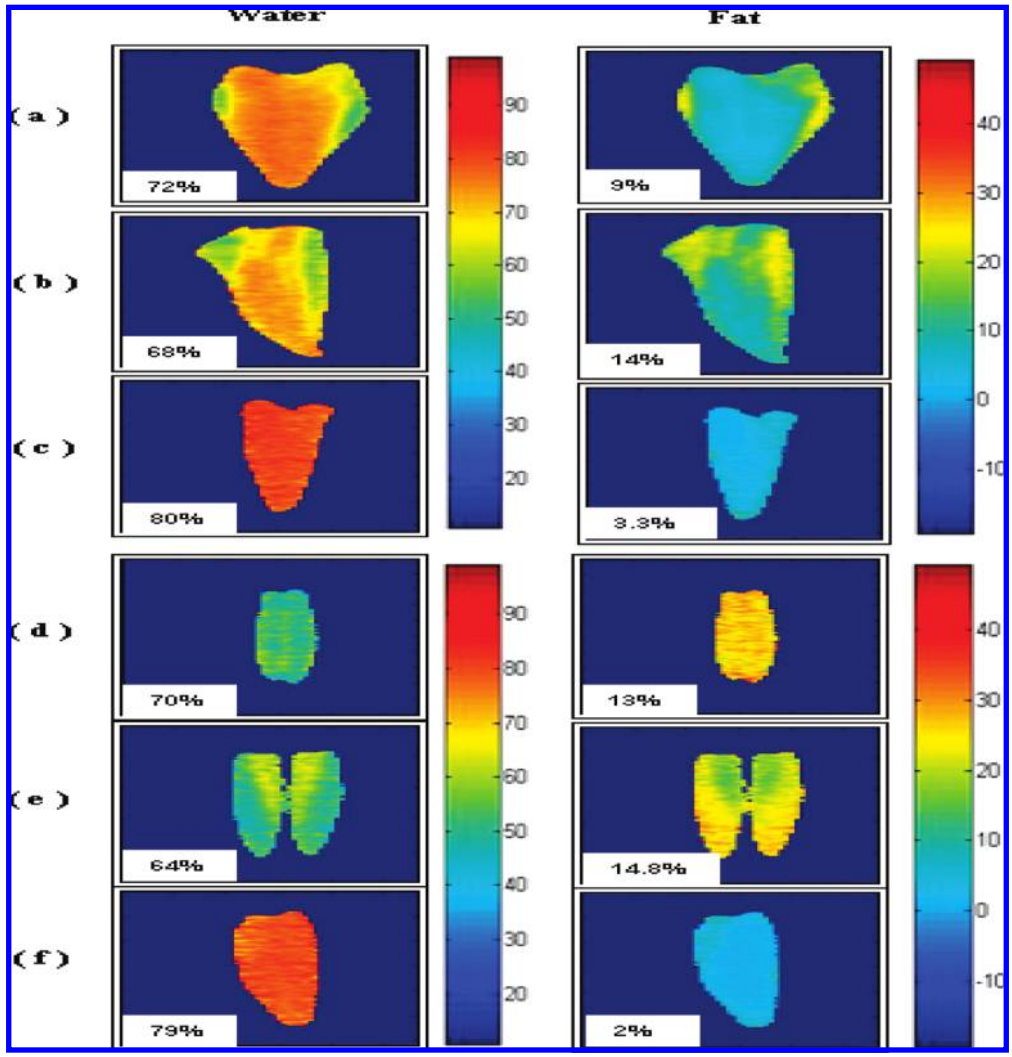

Figure 5. Water and fat distribution maps in fillets of (**a**) Atlantic halibut, (**b**) catfish, (**c**) cod, (**d**) herring, (**e**) mackerel, and (**f**) saithe. The values in the left bottom corner of the figure represent the average concentrations of water and fat in the whole fillet.

and a small difference between RMSEC and RMSECV. It is clear that the PLSR models have high performance in the calibration and validation sets. Water content could be predicted accurately (compared to the reference destructive NMR method) by the PLSR model of eight latent variables with a correlation coefficient of 0.94, RMSEC of 2.45%, and RMSECV of 2.73%. Similarly, a good PLS model of six latent variables was obtained for predicting fat content with a correlation coefficient of 0.91, RMSEC of 2.70%, and RMSECV of 2.99%. The obtained models confirm the suitability of this approach for fat and water prediction. To validate and further refine the models for practical use, more samples of the same or similar species should be included in the calibration to account for more variability in chemical composition and biological variation.

There has been reported more accurate calibrations for fat and water in fish based on NIR analysis (*25, 26*). In those cases, the models are often based on ground meat, or well-defined intact samples, and an optimal match between the NIR measurement and the reference measurement. In our case there is an uncertainty in matching of the extracted spectra and the position of the actual reference subsamples. The main sampling depth of the optical system is down to approximately 15 mm, while the thickness of the cylindrical subsamples varied between about 5 to 20 mm due to different fillet thickness. This will probably introduce some kind of noise in the data. Another complicating factor is the inclusion of different fish species in the same model. They have different optical properties, are of different thickness, and are to some extent different in color. This will add complexity to the model and might be the reason for the high number of PLS factors needed in the models. Better models might be obtained for single species; however, the present result illustrates that a multispecies model is feasible, and in a practical industrial setting, this would be convenient.

Mapping of Water and Fat Distribution. Chemical images for all species are shown in **Figure 5**. The changes in fat and water contents were assigned with a linear color scale. The negative value in the color scale of the fat map is to make the background contrasted to the fillet. Although it was impossible to differentiate the fat and water distribution in the fillet by the naked eye, the spatial distribution of water and fat could be visualized by the NIR interactance imaging system.

It is clear to figure out how the concentrations of fat and water vary drastically between different parts of the same fillet. For instance, in Atlantic halibut the water content in the thick loin of the fillet was much higher than that in the fillet rims and in the belly (**Figure 5a**). Correspondingly, the fat distribution map reveals that the fat content in the rims and in the belly area was higher than that in the middle part. Images like this enable the fish industry to sort fish according to fat content and also cut the fillets according to certain fat thresholds if desired.

A similar result is shown for the catfish fillets shown in **Figure 5b**. The water and fat distribution in cod and saithe fillets

were homogenously distributed, and the difference in fat and water content from pixel to pixel was quite small. This result was confirmed by low standard deviation (SD) values of water and fat contents in these species (**Table 1**).

Although the average fat content in Herring fillets is quite high (13%), it was distributed homogenously in the fillet as illustrated in **Figure 5d**. The homogeneous distribution of a certain constituent will facilitate the work of fish industries if they need to put a reliable documentation of the chemical composition of their products, which will help in differentiating the prices of the final products. Finally, the fat and water in case of mackerel fillets (**Figure 5e**) were distributed in a different manner since only the belly part contains very high fat content compared with the other parts of the fillet. In brief, these chemical images obtained from the online NIR spectral imaging unit explain to a great extent the robustness of the calibration models and the validity of this technique to visualize the water and fat distribution in fish fillets. The results suggest that NIR spectral imaging could become a useful tool for evaluating the distribution of not only water and fat contents in fish fillet but also other important constituents such as protein.

These results confirmed that the 760−1040 nm NIR region is well suited for estimating water and fat in fish fillets. The fillet industry can benefit from the possibility of performing this nondestructive technique at an early stage of processing without additional laborious chemical analysis. This enables early sorting of products and thereby improved quality management. Also, fish manufacturers who wish to cut away fillets with certain threshold concentrations could perform this task easily with limited modification in their production lines. The technique can be implemented as a key component of computer-integrated manufacturing and provide smart opportunities for various applications, not only in fish fillet industries but also in various food quality monitoring processes. The wide application of this automated system would seem to offer a number of potential advantages, including reduced labor costs, the elimination of human error and/or subjective judgment, and the creation of product data in a real time for documentation, traceability, and labeling.

ACKNOWLEDGMENT

We gratefully acknowledge excellent technical assistance from Karen Wahlstrøm Sanden.

LITERATURE CITED

(1) Bykowski, P.; Dutkiewicz, D. Freshwater fish processing and equipment in small plants. FAO Fisheries Circular, No. 905; FAO, Rome, 1996.

(2) FAO. The state of world fisheries and aquaculture; 1998, ISBN: 925104187.

(3) Scatter, C. N. G. Non-destructive spectroscopic techniques for the measurement of food quality. *Trends Food Sci. Technol.* **1997**, *81*, 285–292.

(4) Pasquini, C. Near Infrared Spectroscopy: Fundamentals, Practical Aspects and Analytical Applications. *J. Braz. Chem. Soc* **2003**, *14*, 198–219.

(5) Garini, Y.; Young, I. T.; McNamara, G. Spectral Imaging: Principles and Applications. *Cytometry* **2006**, *69A*, 735–747.

(6) Cen, H.; He, Y. Theory and application of near infrared reflectance spectroscopy in determination of food quality. *Trends Food Sci. Technol.* **2007**, *18*, 72–83.

(7) Nortvedt, R.; Torrissen, O. J.; Tuene, S. Application of near-infrared transmittance spectroscopy in the determination of fat, protein and dry matter in Atlantic halibut fillet. *Chemom. Intell. Lab. Syst.* **1998**, *42*, 199–207.

(8) Heia, K.; Sivertsen, A. H.; Stormo, S. K.; Elvevoll, E.; Wold, J. P.; Nilsen, H. Detection of Nematodes in Cod (*Gadus morhua*) Fillets by Imaging Spectroscopy. *J. Food Sci.* **2007**, *72*, E11−E15.

(9) ElMasry, G.; Wang, N.; Vigneault, C.; Qiao, J.; ElSayed, A. Early detection of apple bruises on different background colors using hyperspectral imaging. *LWT−Food Sci. Technol.* **2008**, *41*, 337–345.

(10) Wold, J. P.; Johansen, T.; Haugholt, K. H.; Tschudi, J.; Thielemann, J.; Segtnan, V. H.; Narum, B.; Wold, E. Non-contact transflectance near infrared imaging for representative on-line sampling of dried salted coalfish (bacalao). *J. Near Infrared Spectrosc.* **2006**, *14*, 59–66.

(11) Chao, K.; Chen, Y. R.; Hruschka, W. R.; Park, B. Chicken heart disease characterization by multi-spectral imaging. *Trans. ASAE* **2001**, *17*, 99–106.

(12) Park, B.; Windham, W. R.; Lawrence, K. C.; Smith, D. P. Hyperspectral image classification for fecal and ingesta identification by spectral angle mapper. Presented at the ASAE/CSAE Meeting, Ottawa, Ontario, Canada, 2004, ASAE Paper No. 043032.

(13) Polder, G.; Van der Heijden, G.W.A. M.; Young, I. T. Spectral image analysis for measuring ripeness of tomatoes. *Trans. ASAE* **2002**, *45*, 1155–1161.

(14) Cheng, X.; Chen, Y. R.; Tao, Y.; Wang, C. Y.; Kim, M. S.; Lefcourt, A. M. A novel integrated PCA and FLD method on hyperspectral image feature extraction for cucumber chilling damage inspection. *Trans. ASAE* **2004**, *47*, 1313–1320.

(15) Liu, Y.; Chen, Y. R.; Wang, C. Y.; Chan, D. E.; Kim, M. S. Development of hyperspectral imaging technique for the detection of chilling injury in cucumbers; spectral and image analysis. *Appl. Eng. Agric.* **2006**, *22*, 101–111.

(16) ElMasry, G.; Wang, N.; ElSayed, A.; Ngadi, M. Hyperspectral imaging for nondestructive determination of some quality attributes for strawberry. *J. Food Eng.* **2007**, *81*, 98–107.

(17) Tsuta, M.; Takao, T.; Sugiyama, J.; Wada, Y.; Sagara, Y. Foreign Substance Detection in Blueberry Fruits by Spectral Imaging. *Food Sci. Technol. Res* **2006**, *12*, 96–100.

(18) Sugiyama, J. Visualization of Sugar Content in the Flesh of a Melon by Near-Infrared Imaging. *J. Agric. Food Chem.* **1999**, *47*, 2715–2718.

(19) Tsuta, M.; Sugiyama, J.; Sagara, Y. Near-Infrared Imaging Spectroscopy Based on Sugar Absorption Band for Melons. *J. Agric. Food Chem.* **2002**, *50*, 48–52.

(20) Mehl, P. M.; Chao, K.; Kim, M.; Chen, Y. R. Detection of defects on selected apple cultivars using hyperspectral and multispectral image analysis. *Appl. Eng. Agric.* **2002**, *18*, 219–226.

(21) Lee, K. J.; Kang, S.; Kim, M. S.; Noh, S. H. Hyperspectral imaging for detecting defect on apples. Presented at the Annual Meeting of ASAE, Tampa, FL, July 17−20, 2005, ASAE Paper No. 053075.

(22) Bencze Røra, A. M.; Kvåle, A.; Mørkøre, T.; Rørvik, K. A.; Steien, S. H.; Thomassen, M. S. Process yield, colour and sensory quality of smoked Atlantic salmon (Salmon salar) in relation to raw material characteristics. *Food Res. Int.* **1998**, *31*, 601–609.

(23) Sørland, G. H.; Larsena, P. M.; Lundby, F. Determination of total fat and moisture content in meat using low field NMR. *Meat Sci.* **2004**, *66*, 543–550.

(24) Osborne, B. G.; Fearn, T. *Near-Infrared Spectroscopy in Food Analysis*; Wiley: New York, 1988.

(25) Wold, J. P.; Jakobsen, T.; Krane, L. Atlantic Salmon Average Fat Content Estimated By Near-Infrared Transmittance Spectroscopy. *J. Food Sci.* **1996**, *61*, 74–77.

(26) Sollied, H.; Solberg, C. Salmon fat content estimation by near-infrared transmission spectroscopy. *J. Food Sci.* **1992**, *57*, 792–793.

Received for review April 4, 2008. Revised manuscript received June 15, 2008. Accepted June 17, 2008. We gratefully acknowledge financial support from the Norwegian Research Council.

JF801074S